RSC Applied Polymers

ROYAL SOCIETY OF CHEMISTRY

PAPER

View Article Online
View Journal | View Issue

Cite this: *RSC Appl. Polym.*, 2025, **3**, 651

Cationic nano-objects produced by polymerization-induced self-assembly using sulfonium-macro chain transfer agents with different counter anions†

Hirotsugu Miyakawa and Hideharu Mori *

Sulfonium cations and sulfonium-based polymers have received increased interest as biomedical and ion-conductive materials because of their unique cationic features. However, the feasible construction of cationic nanostructures *via* polymerization-induced self-assembly (PISA) remains limited owing to charge repulsion. In this study, we report the efficient synthesis of sulfonium cation-based nano-objects from P(MTEA(S^+)[R^-])s with different counter anions (R = bis(trifluoromethylsulfonyl)imide, TFSI; trifluoromethanesulfonate, OTf; and chloride, Cl), which were prepared by reversible addition–fragmentation chain-transfer (RAFT) of 2-(methylthio)ethyl acylate (MTEA) and a subsequent anion exchange reaction. RAFT dispersion copolymerization of styrene (St) and *N*-phenylmaleimide (PMI) using cationic P(MTEA(S^+)[R^-]) macro-chain transfer agents (CTAs) afforded various assembled structures (worms, vesicles, and nanotubes) by tuning the chain lengths of the P(MTEA(S^+)[R^-]) and P(St-*alt*-PMI) blocks and their composition and polymerization conditions (*e.g.*, monomer concentration and solvent polarity). Depending on the three cationic macro-CTAs, the PISA of St and PMI enabled the efficient copolymerization and construction of cationic assemblies, including unique nanotubes. This is the first study demonstrating the successful integration of the sulfonium macro-CTA and PISA, enabling the design and manipulation of cationic nano-objects with various morphologies and unique functionalities originating from sulfonium cations.

Received 16th January 2025,
Accepted 4th March 2025

DOI: 10.1039/d5lp00009b

rsc.li/rscapplpolym

Introduction

Polymerization-induced self-assembly (PISA) has been developed as an efficient methodology to manipulate the morphologies of self-assembled block copolymers by tuning chemical structures (*e.g.*, the structure of the solvophilic/solvophobic blocks and their composition) and selecting suitable conditions (*e.g.*, solvent polarity and concentration).[1–13] PISA enables the feasible creation of versatile ordered structures (*e.g.*, spheres, worms, vesicles, and nanotubes) in one step at high concentration.[1,14–21] Emulsion and dispersion polymerizations *via* the reversible addition–fragmentation chain-transfer (RAFT) process have been widely employed to produce nano-objects *via* PISA.[2,3,5,7,12] In addition to the feasibility to manipulate self-assembled architectures, increasing attention has been recently paid to the incorporation of reactive and functional units *via* PISA, which is crucial for diverse potential applications.[1,3,11,22] The rational design of the macro-chain transfer agent (macro-CTA) is essential, as it can be used as a stabilizing block during PISA and generates functional units on the shell of the polymeric nano-objects after polymerization. Although various functional macro-CTAs (*e.g.*, non-ionic and ionic CTAs) have been developed as stabilizing blocks for block copolymer assemblies with shell-functionalities,[1,3,11,22] the feasible construction of cationic and anionic nanostructures is still limited. Owing to the decrease in packing parameters caused by charge repulsion, only a spherical structure, the so-called kinetically trapped morphology,[3,11] has been observed. To access higher-ordered structures (*e.g.*, worm and vesicles), several approaches have been proposed, which include (1) using a copolymer-type macro-CTA consisting of cationic and non-ionic monomers,[23] (2) mixing cationic and non-ionic macro-CTAs,[23,24] and (3) adding a suitable salt to screen the charge.[25,26]

Ionic liquid-type macro-CTAs, such as imidazolium,[27–29] phosphonium,[30] and diallyldimethylammonium[31] salt-containing polymers, have been employed to afford cationic nano-objects, showing morphological evolution in some systems.

Department of Organic Materials Science, Graduate School of Organic Materials Science, Yamagata University, 4-3-16, Jonan, Yonezawa City, Yamagata Prefecture 992-8510, Japan. E-mail: h.mori@yz.yamagata-u.ac.jp

† Electronic supplementary information (ESI) available. See DOI: https://doi.org/10.1039/d5lp00009b

For instance, Bernard *et al.* reported the formation of poly (ionic liquid)-based nano-objects involving vesicles and worms by RAFT polymerization of 4-vinyl pyridine using an imidazolium salt-containing macro-CTA.[27] Since the solubilities and unique cationic features of ionic liquids can be tuned by the structures of the cationic species, counter ions, and substituent groups, a variety of ionic liquid-based nano-objects have been developed by PISA, which include all poly(ionic liquid) block copolymer nano-objects,[28,32,33] homopolymer nanovesicles,[34] and block copolymer nano-objects with ionic liquid-based cores.[35,36] Some of these poly(ionic liquid)-based assemblies afforded morphological transformations (*e.g.*, from spheres to rods and vesicles[28]). However, a comprehensive understanding of the structural transitions of cationic nano-objects and the essential parameters affecting their morphological evolution is highly desirable. In addition to PISA, a variety of block copolymers consisting of poly(ionic liquid)s have been developed by controlled polymerization techniques[37] and used to form various nanostructures in film[38–41] and solution states.[42–44] Unique poly(ionic liquid)-based block copolymer assemblies may be governed by a suitable section of the cation/anion combination, which can weaken the ion pair coordination, reduce intermolecular interactions, and break the symmetry of their chemical structures, in addition to the essential parameters (*e.g.*, block lengths and composition) of traditional block copolymer assemblies.[45]

Nanotube formation and polymersome growth *via* PISA have attracted great interest owing to their potential for biomedical and nanotechnological applications and unique shapes with large aspect ratios; however, only limited systems have yet been achieved.[17,18,46–53] In reported mechanisms, the restriction of chain mobility was demonstrated to be essential to achieve 1D vesicle fusion to produce nanotubes. Various approaches have been proposed to realize polymeric nanotube formation, such as enhanced rigidity by selecting core-forming blocks with high glass transition temperatures,[48,51] employment of aromatic interactions between solvophobic blocks[50,53] and hydrogen bonding in the core part,[18] and polymerization at low temperature[52] and in viscous poly(ethylene glycol) medium.[17] Despite recent advances in sophisticated strategies for constructing polymeric nanotubes and polymersomes, feasible modifications of the surface and interior of polymeric nanotubes and manipulation of their three-dimensional structures (*e.g.*, aspect ratios, outer shell diameters, and interior holes) remain challenging. In particular, cationic polymeric tubes with adjustable three-dimensional structures and large aspect ratios have not been reported.

Herein, we report the synthesis of cationic nano-objects with structural evolution (worms, vesicles, and nanotubes) by PISA *via* RAFT dispersion polymerization using sulfonium cation-containing macro-CTAs (Fig. 1). Sulfonium cations and sulfonium-based polymers have received increased interest as biomedical and ion-conductive materials because of their unique cationic features (*e.g.*, relatively low viscosities),[54] high ionic conductivity,[55–58] intrinsic ability to form a polyplex with nucleic acid,[59,60] and antibacterial properties.[61,62] We focused on the manipulation of the morphologies of cationic nano-objects using sulfonium macro-CTAs, P(MTEA(S^+)[R^-])s, with different counter anions (R = bis(trifluoromethylsulfonyl) imide, TFSI; trifluoromethanesulfonate, OTf; and chloride, Cl). These anions are frequently employed as a component for ionic liquids, and they have different sizes ($TFSI^-$ > OTf^- > Cl^-), properties (*e.g.*, $TFSI^-$ has low electronegativity to form ion pairs with soft cations and Cl^- has high electronegativity to act as a highly ionized ion, belonging to soft and hard anions, respectively), and ability to tune the solubility (*e.g.*, hydrophobic $TFSI^-$ is used to afford a water-insoluble cationic block).[42,44,63–66] A thioether unit in the polymer (PMTEA) prepared from 2-(methylthio)ethyl acylate (MTEA) was used to introduce sites for cationization and the subsequent anion exchange reaction, enabling manipulation of the nature of the sulfonium cation-containing segments. Furthermore, P(MTEA(S^+)[R^-])s acted as a stabilizing block during RAFT-PISA and functionalized shell parts in the resulting cationic nano-objects. The RAFT dispersion polymerization of styrene (St) and *N*-phenylmaleimide (PMI) using P(MTEA(S^+)[$TFSI^-$]) was investigated by varying the monomer concentration and polymerization time to determine the optimal conditions for the construction of cationic nano-objects with various morphologies. Structural transformations of the assembled structures were evaluated using transmission electron microscopy (TEM) and dynamic light scattering (DLS). Subsequently, the effect of the counterions (R = TFSI, OTf, and Cl) of the sulfonium macro-CTAs on the morphology was investigated. Sulfonium cation-based nanotubes were obtained by tuning the solvophilic/solvophobic balance using the monomer (St + PMI)/macro-CTA feed ratio. These findings demonstrate a promising pathway for design of cationic nano-objects deco-

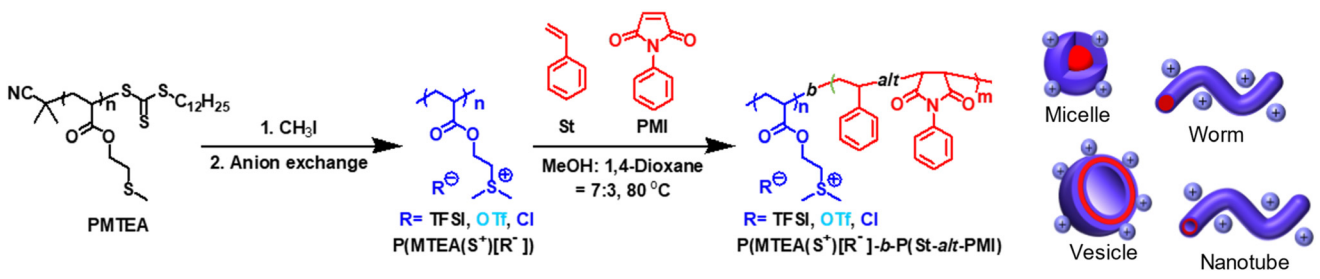

Fig. 1 Synthesis of sulfonium-based nano-objects by RAFT-PISA using P(MTEA(S^+)[R^-]).

rated with sulfonium-type poly(ionic liquid)s for various potential applications, such as ionic conductive materials,[67] organic thin-film transistors,[68] and gene delivery systems.[59,69]

Results and discussion

Preparation of sulfonium macro-CTAs having different counterions

The synthesis pathway used for the production of cationic nano-objects is illustrated in Fig. 1. Three P(MTEA(S^+)[R^-])s with different counter anions (R = TFSI, OTf, and Cl) were synthesized and used as sulfonium macro-CTAs for RAFT-PISA. Initially, a non-ionic precursor (PMTEA) with predetermined molecular weights ($M_{n,NMR}$ = 7300, $M_{n,SEC}$ = 7000, M_w/M_n = 1.18) was synthesized *via* the RAFT polymerization of MTEA with a trithiocarbonate-type CTA (Table S2 and Fig. S3†). The cationization of the thioether unit in the PMTEA side chain was conducted using methyl iodide as reported previously,[60] and the subsequent anion exchange reaction with lithium and sodium salts (LiTFSI, LiOTf, and NaCl) afforded P(MTEA(S^+)[$TFSI^-$]), P(MTEA(S^+)[OTf^-]), and P(MTEA(S^+)[Cl^-]), respectively (Table S5†). The quantitative transformation of the non-ionic PMTEA into cationic polymers with different counter anions was confirmed by ^{1}H NMR analysis. After the cationization, the ^{1}H NMR signals attributed to the MTEA unit at 4.2–4.1, 2.8–2.7, and 2.2–2.1 ppm disappeared in all the cases (Fig. 2). Alternatively, new peaks at 4.5–4.3, 3.7–3.5, and 3.0–2.9 ppm, corresponding to –COO–CH_2–, –CH_2–S^+–, and –S^+–(CH_3)$_2$ units, were visible for P(MTEA(S^+)[$TFSI^-$]) in DMSO-d_6. Similarly, new peaks at 4.7–4.5, 3.9–3.7, and 3.2–2.9 ppm were detected for P(MTEA(S^+)[OTf^-]) and P(MTEA(S^+)[Cl^-]) in D_2O.

Three sulfonium macro-CTAs, P(MTEA(S^+)[R^-])s, were soluble in methanol but insoluble in 1,4-dioxane, regardless of the counterions (R = TFSI, OTf, and Cl), as shown in Table S6.† Note that P(MTEA(S^+)[OTf^-]) and P(MTEA(S^+)[Cl^-]) were soluble in water but insoluble in chloroform, while P(MTEA(S^+)[$TFSI^-$]) was soluble in chloroform and DMSO, but insoluble in water, suggesting that P(MTEA(S^+)[OTf^-]) and P(MTEA(S^+)[Cl^-]) are more hydrophilic than P(MTEA(S^+)[$TFSI^-$]). The different polarities of the sulfonium macro-CTAs may affect their self-assembly behavior *via* PISA.

RAFT-PISA using P(MTEA(S^+)[$TFSI^-$]) as a sulfonium macro-CTA

P(MTEA(S^+)[$TFSI^-$]) was used as a sulfonium macro-CTA for the construction of cationic nano-objects with various morphologies. Initially, St was polymerized using 2,2′-azobis(isobutyronitrile) (AIBN) with the P(MTEA(S^+)[$TFSI^-$]) macro-CTA at [AIBN]/[macro-CTA]/[St] = 1/5/1000–10 000 in methanol (Table S7†). P(MTEA(S^+)[$TFSI^-$])-*b*-PSts were obtained with reasonable conversions (40–83%) at 80 °C after 48 h. However, almost spheres were obtained (Fig. 3 and S4†), implying a kinetically trapped morphology, regardless of the PSt chain length (degree of polymerization (DP) = 123–2464) for PSt, compared to 48 for P(MTEA(S^+)[$TFSI^-$]).

Next, RAFT copolymerization of St and PMI was examined because alternating copolymerization is preferable for achieving high yield polymeric products, and the rigidity of the P(St-

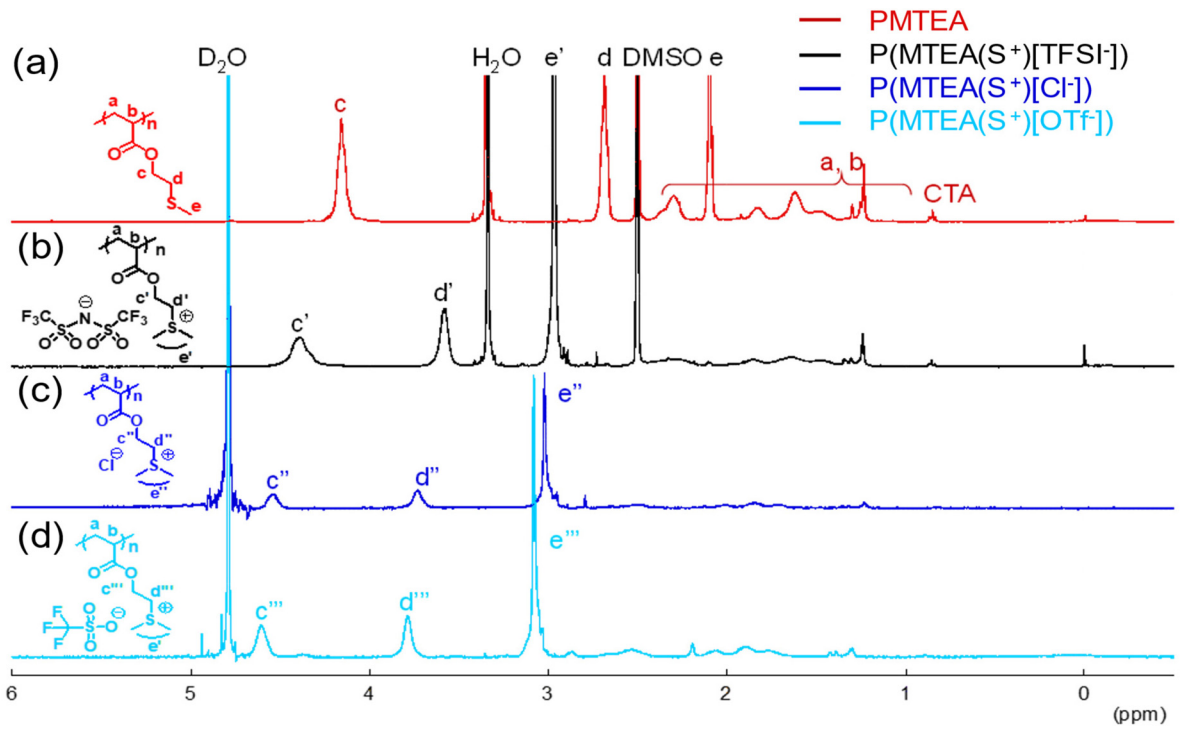

Fig. 2 ^{1}H NMR spectra of (a) PMTEA in DMSO-d_6 (b) P(MTEA(S^+)[$TFSI^-$]) in DMSO-d_6, (c) P(MTEA(S^+)[Cl^-]) in D_2O and (d) P(MTEA(S^+)[OTf^-]) in D_2O.

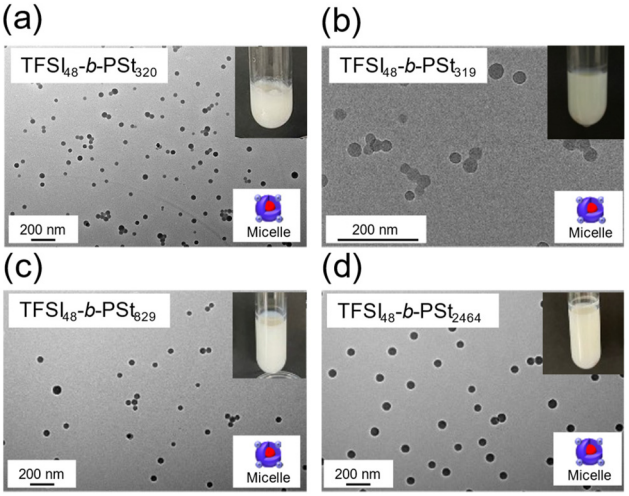

Fig. 3 TEM images of P(MTEA(S^+)[$TFSI^-$])-*b*-PSts obtained by RAFT-PISA at [AIBN]/[macro-CTA]/[St] = 1/5/1000–10 000 (solid content = 20 wt%) using P(MTEA(S^+)[$TFSI^-$]) macro-CTA (M_n = 21 500) for (a) 24 h and (b–d) 48 h.

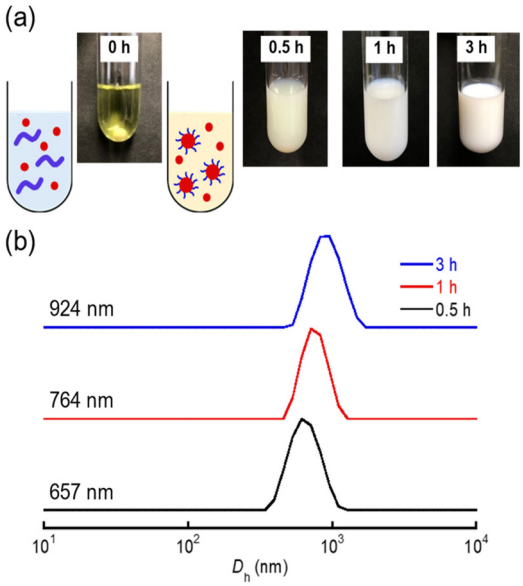

Fig. 4 (a) Turbidity changes and (b) DLS traces of P(MTEA(S^+)[$TFSI^-$])-*b*-P(St-*alt*-PMI)s prepared by RAFT-PISA at [AIBN]/[macro-CTA]/[St]/[PMI] = 1/5/1000/1000, solvent = methanol/1,4-dioxane = 7/3 (wt/wt, solid content = 5 wt%).

alt-PMI) segment (high glass transition temperatures) can contribute to the formation of sheet-like two dimensional structures.[49,70] The copolymerization was conducted with AIBN in methanol/1,4-dioxane (7/3, wt/wt) at 80 °C. Methanol was a good solvent for P(MTEA(S^+)[$TFSI^-$]), St, and PMI, while P(St-*alt*-PMI) was soluble in 1,4-dioxane and insoluble in methanol. When copolymerization was performed for [AIBN]/[macro-CTA]/[St]/[PMI] = 1/5/1000/1000 at a low concentration (solid content = 5 wt%), the transparent solution gradually turned into a white dispersion with increasing polymerization time (0.5, 1, and 3 h) (Fig. 4a). An initial increase in the monomer conversion was detected after 0.5 h (27%), followed by plateau (84, and 89% for 1 and 3 h), as monitored by ^{1}H NMR spectroscopy (Table 1). The chemical structure and composition of P(MTEA(S^+)[$TFSI^-$])-*b*-P(St-*alt*-PMI)s were confirmed by ^{1}H NMR in $CDCl_3$/DMSO-d_6 (1/1 vol%, Fig. S7†). The molecular weights of P(MTEA(S^+)[$TFSI^-$])-*b*-P(St-*alt*-PMI)s calculated from ^{1}H NMR increased from 34 000 to 62 000, whereas the DP of the core-forming P(St-*alt*-PMI)s increased from 46 to 148, compared to 48 for P(MTEA(S^+)[$TFSI^-$]) (Table 1). The copolymer structure was also analyzed using diffusion-ordered NMR spectroscopy (DOSY). P(MTEA(S^+)[$TFSI^-$])-*b*-P(St-*alt*-PMI) showed the same diffusion coefficient for the DOSY NMR signals from both P(St-*alt*-PMI) and P(MTEA(S^+)[$TFSI^-$]) segments (Fig. S8 and S9†), implying the formation of the block copolymer. Therefore, PISA processes using St and PMI in the presence of the sulfonium macro-CTA in methanol/1,4-dioxane (7/3, wt/wt) at 5 wt% prompted the search for suitable reaction parameters to obtain high monomer conversion with a predetermined hydrophilic/hydrophobic balance. A similar kinetic behavior and an increase in the chain length of P(St-*alt*-PMI)s with polymerization time were observed at higher monomer concentrations (solid contents = 10 and 20 wt%, Fig. S10†). The resulting P(MTEA(S^+)[$TFSI^-$])-*b*-P(St-*alt*-PMI)s exhibited tunable molecular weights ($M_{n,NMR}$ = 35 000–71 000) and monomer compositions (P(St-*alt*-PMI)s: 49–158 and 112–182, compared to 48 for P(MTEA(S^+)[$TFSI^-$])). These results imply efficient chain extension of the P(MTEA(S^+)[$TFSI^-$]) with St and PMI with increasing monomer conversion to afford P(MTEA(S^+)[$TFSI^-$])-*b*-P(St-*alt*-PMI)s with predetermined composition of cationic P(MTEA(S^+)[$TFSI^-$]) and hydrophobic P(St-*alt*-PMI) chains.

The assembled structures of P(MTEA(S^+)[$TFSI^-$])-*b*-P(St-*alt*-PMI)s prepared under various conditions were evaluated by TEM and DLS. Initially, TEM images were employed without staining to visualize the morphologies, in which the dark areas can be attributed to the cationic P(MTEA(S^+)[R^-]) block consisting of the sulfonium cation/TFSI anion ion pairs, leading to a higher electron density compared to the hydrophobic P(St-*alt*-PMI) block. The stain-free TEM images of the P(MTEA(S^+)[$TFSI^-$])-*b*-P(St-*alt*-PMI)s assemblies prepared *via* PISA at a low concentration (5 wt%) after 0.5 h showed worms and vesicles with some defects, which were slightly changed into stable assemblies maintaining the worm and vesicle structures up to 3 h (Fig. 5). The intensity-averaged hydrodynamic diameters evaluated by DLS measurements indicated a gradual increase in the particle size (657, 764, and 924 nm) from 0.5 to 3 h (Fig. 4b). The zeta potentials were 30–38 mV, implying the presence of the cationic P(MTEA(S^+)[$TFSI^-$]) on the surface of the block copolymer assemblies.

A remarkable effect of the monomer concentration on the assembly of P(MTEA(S^+)[$TFSI^-$])-*b*-P(St-*alt*-PMI)s was observed. At an intermediate concentration (10 wt%), the worm-like structures observed after 0.5 h were changed into small vesicles that were partially connected to each other after 1 h and

Table 1 Synthesis of P(MTEA(S^+)[$TFSI^-$])-*b*-P(St-*alt*-PMI)s by RAFT-PISA at 80 °C[a]

Run	Time (h)	Solid (wt%)	Conv.[b] (%)	Yield[c] (%)	M_n [b] (^{1}H NMR)	n : m[b]	D_h [d] (nm)	Zeta potential (mV)	Morphology[e]
1	0.5	5	27	22	34 000	48 : 46	657	+34.2	W, V
2	1		84	63	55 000	48 : 123	764	+38.0	W, V
3	3		89	64	62 000	48 : 148	924	+30.0	W, V
4	0.5	10	13	29	35 000	48 : 49	255	+30.8	W
5	1		92	34	54 000	48 : 120	241	+31.4	V
6	3		93	30	65 000	48 : 158	323	+43.3	V
7	0.5	20	65	51	52 000	48 : 112	155	+32.3	M, W
8	1		94	56	64 000	48 : 154	720	+29.5	V
9	3		92	77	71 000	48 : 182	268	+43.4	V

[a] [AIBN]/[macro-CTA]/[St]/[PMI] = 1/5/1000/1000, P(MTEA(S^+)[$TFSI^-$]) macro-CTA: M_n = 21 500, solvent = methanol : 1,4-dioxane = 7 : 3 (w/w, solid content = 5–20 wt%). [b] Calculated by ^{1}H NMR in $CDCl_3$: DMSO-d_6 = 1 : 1. [c] Dialysis in MeOH for 3 days. [d] Measured by DLS in MeOH. [e] Morphology was determined by TEM, where M, micelle; W, worm; V, vesicle.

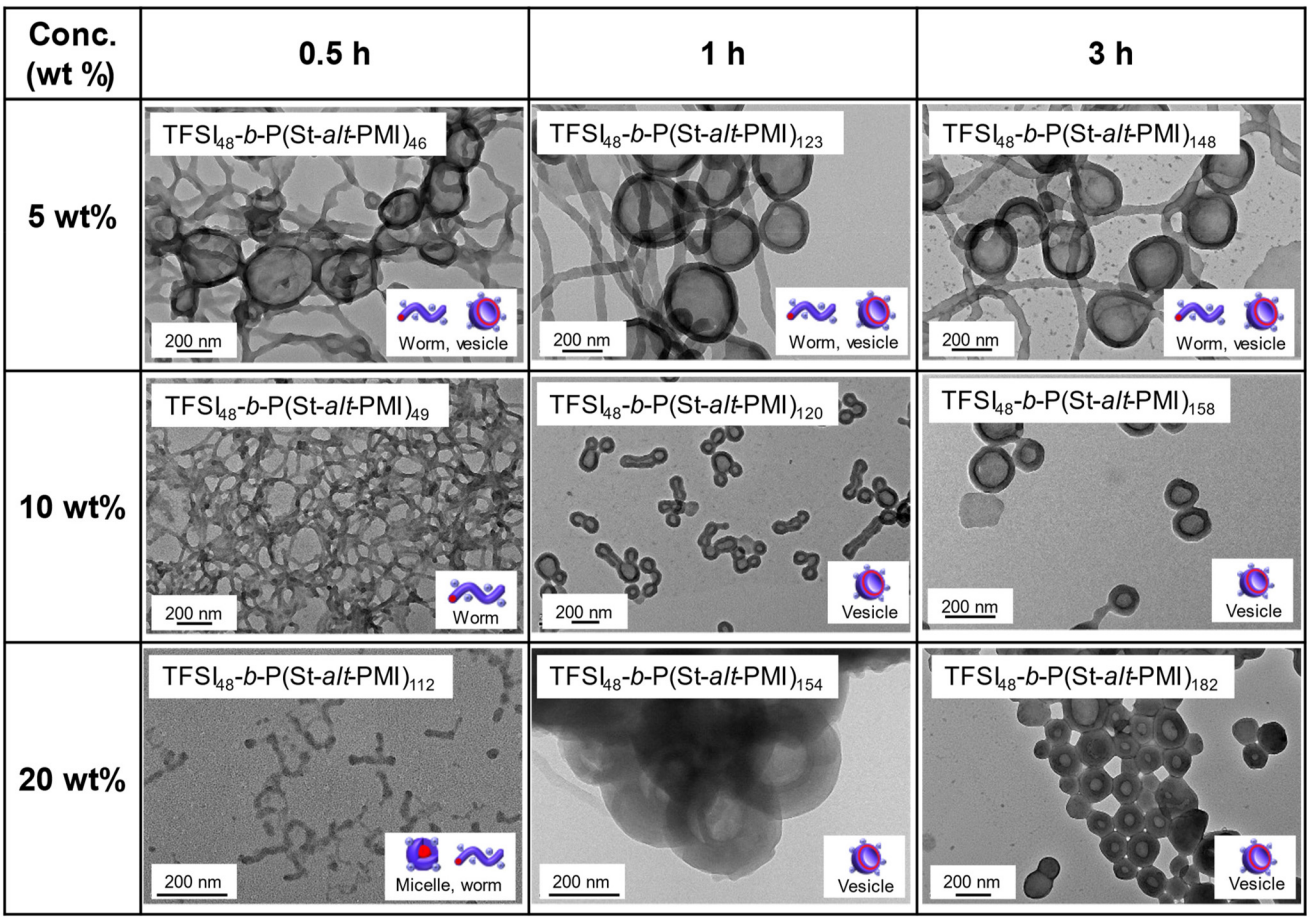

Fig. 5 TEM images of P(MTEA(S^+)[$TFSI^-$])-*b*-P(St-*alt*-PMI)s obtained by RAFT-PISA at [AIBN]/[macro-CTA]/[St]/[PMI] = 1/5/1000/1000 (solid content = 5–20 wt%) using P(MTEA(S^+)[$TFSI^-$]) macro-CTA (M_n = 21 500).

large spherical vesicles (>200 nm) after 3 h, which were detected by TEM (Fig. 5). DLS studies indicated the formation of assemblies with a broad size distribution (D_h = 255 nm) after 0.5 h, which changed into assemblies with narrower distributions with slight changes over time (D_h = 241 and 323 nm after 1 and 3 h, respectively). At a higher concentration (20 wt%), a clear morphological transformation was detected from small micelles mixed with worms at 0.5 h into large vesicles with thicker shells at 1 and 3 h (Fig. 5). The DLS results indicated a drastic increase in the size of P(MTEA(S^+)[$TFSI^-$])-*b*-P(St-*alt*-PMI) assemblies obtained after 0.5 h (D_h = 155 nm) into that after 1 h (D_h = 720 nm), followed by a decrease in size

after 3 h (D_h = 268 nm, Fig. S11†). In all cases, a substantial change in the size and morphology of the assembled structures with increasing polymerization time was observed by DLS and TEM measurements while maintaining positive charges (29–44 mV). This behavior was distinct from that of conventional cationic macro-CTAs, in which a positive charge on the initial assembled structures suppresses further morphological changes.

Interestingly, nanotube-like structures with hollow channels covered with dark walls were observed in the case of a prolonged polymerization time (6 h) at a higher concentration (20 wt%), as shown in Fig. 6a, b and S12a, b.† Occasionally, vesicles sticking to the wall of the nanotube were visible. The length of the P(MTEA(S^+)[$TFSI^-$])$_{48}$-*b*-P(St-*alt*-PMI)$_{197}$ nanotubes exceeded one micrometer (≥1 μm) with a diameter of 70–120 nm and wall thickness of 25–30 nm, and the size of the vesicles ranged from 80 to 100 nm. A further increase in the polymerization time (24 h) led to the predominant formation of similar nanotube-like structures mixed with a small number of vesicles (Fig. 6c, d, Fig. S12c, d, and Table S8†). The positive charge (approximately 26–37 mV) was maintained on the assembled structures, implying the feasibility of the structural transformation even if the cationic P(MTEA(S^+)[$TFSI^-$]) existed predominantly on the outermost surface of the assembles. This implies that further morphological changes are not disturbed by the repulsion of the sulfonium macro-CTA, which is distinct from the conventional cationic macro-CTA. Fig. 6e shows a phase diagram for P(MTEA(S^+)[$TFSI^-$])-*b*-P(St-*alt*-PMI) assemblies prepared at different concentrations (solid content = 5, 10, and 20 wt%). Mixed morphologies of worms and vesicles were predominantly observed at a low concentration (5 wt%), suggesting that the limited possibility of the fusion of initially assembled structures inhibited further progress to form higher-ordered structures. In contrast, clear vesicles were observed for the P(MTEA(S^+)[$TFSI^-$])-*b*-P(St-*alt*-PMI)s with long P(St-*alt*-PMI) chains prepared at higher concentrations (10 and 20 wt%). Nanotube-like structures were observed when the DP of the hydrophobic P(St-*alt*-PMI) chain was close to 200, compared to 48 for the cationic P(MTEA(S^+)[$TFSI^-$]) chain. Isolated nanotubes with partially broken and disconnected sections were occasionally observed. Similar to another nanotube formed *via* PISA,[48] the intrinsically brittle structure, which probably originates from the rigid P(St-*alt*-PMI) segment in the present system, may have contributed to breakage along the nanotubes during the drying process for TEM sample preparation. A further increase in the monomer concentration (30 wt%) afforded fused vesicles located at the end-capping part of the short tube-like structure (Fig. S14†), suggesting the progress of one-dimensional fusion from the vesicles, as proposed in the reported nanotube formation mechanism.[48] Therefore, RAFT-PISA of St and PMI was realized using the sulfonium P(MTEA(S^+)[$TFSI^-$]) macro-CTA, enabling the design of cationic assemblies with various morphologies from micelles to nanotubes.

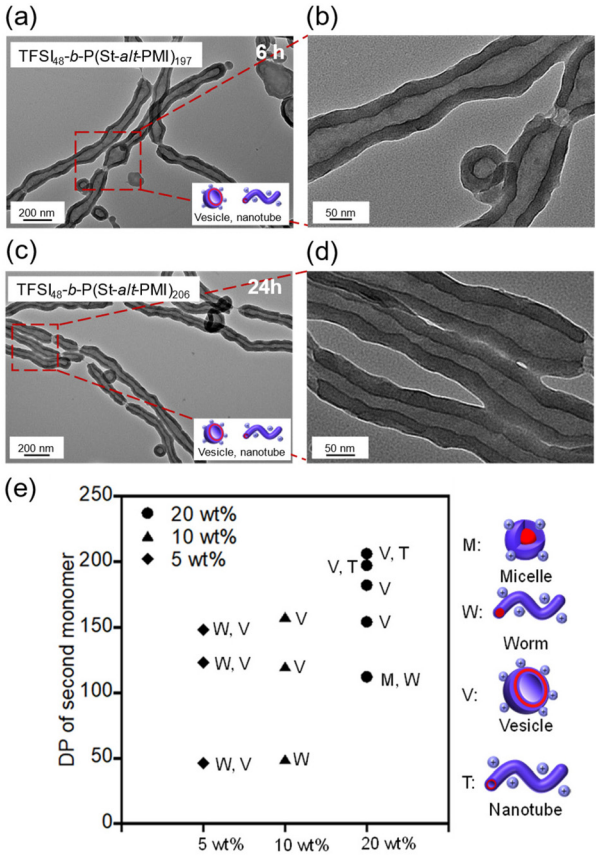

Fig. 6 (a–d) TEM images and (e) phase diagrams constructed of P(MTEA(S^+)[$TFSI^-$])-*b*-P(St-*alt*-PMI)s obtained by RAFT-PISA at [AIBN]/[macro-CTA]/[St]/[PMI] = 1/5/1000/1000 (solid content = 5, 10, and 20 wt%) using P(MTEA(S^+)[$TFSI^-$]) macro-CTA (M_n = 21 500) for (a, b) 6 h and (c and d) 24 h (20 wt%). (e) Morphology was determined by TEM, where M = micelle, W = worm, V = vesicle, and T = nanotube, respectively.

The effect of the solvent polarity on the assembled structures of P(MTEA(S^+)[$TFSI^-$])-*b*-P(St-*alt*-PMI)s was evaluated. When St/PMI was copolymerized with the P(MTEA(S^+)[$TFSI^-$]) macro-CTA in methanol under the same conditions, spherical structures were predominantly observed by TEM (Fig. S16, and Table S10†). Sheet-like structures were obtained by the copolymerization in methanol/1,4-dioxane (9/1, wt/wt), suggesting that the addition of a small amount of 1,4-dioxane to methanol increased the solubility of core-forming P(St-*alt*-PMI), but decreased the solubility of the P(MTEA(S^+)[$TFSI^-$]) macro-CTA, possibly enabling further structural evolution. A suitable solvent polarity of the mixed solvent (methanol/1,4-dioxane = 7/3 wt/wt) for the solvophilic P(MTEA(S^+)[$TFSI^-$]) and solvophobic P(St-*alt*-PMI) is essential to achieve morphological growth of P(MTEA(S^+)[$TFSI^-$])-*b*-P(St-*alt*-PMI) assemblies from micelles into nanotubes.

As another control experiment, a non-ionic PMTEA (before cationization) was used as a macro-CTA to elucidate the effect of P(MTEA(S^+)[$TFSI^-$]) as a sulfonium macro-CTA on the assembled structures formed *via* PISA. RAFT-PISA of St and PMI was conducted using a PMTEA macro-CTA ($M_{n,NMR}$ = 6600, M_w/M_n = 1.18) with [AIBN]/[macro-CTA]/[St]/[PMI] = 1/5/

1000/1000 in methanol/1,4-dioxane (7/3 wt/wt, solid content = 20 wt%) at 80 °C (Table S11†). The progress of the copolymerization and the structure of the resulting PMTEA-*b*-P(St-*alt*-PMI) were confirmed by the turbidity and ^{1}H NMR measurements (Fig. S17†). SEC measurements revealed that the unimodal peak of the PMTEA macro-CTA shifted to a higher molecular weight region without a shoulder or tailing peak (Fig. S18†), implying the formation of PMTEA-*b*-P(St-*alt*-PMI) ($M_{n,SEC}$ = 24 000, M_w/M_n = 1.41). However, no clear assembled structures were detected using TEM (Fig. S19†). These results suggest that the sulfonium macro-CTA, P(MTEA(S^+)[$TFSI^-$]), could promote bridging between the initial assembled structures (*e.g.*, spherical micelles and vesicles) during RAFT-PISA, resulting in the formation of higher-ordered structures.

Structural effect of the sulfonium macro-CTAs having different counter anions

The effect of the counterion (R = TFSI, OTf, and Cl) of the sulfonium macro-CTA on the morphologies of P(MTEA(S^+)[R^-])-*b*-P(St-*alt*-PMI) assemblies were investigated in methanol/1,4-dioxane (7/3, wt/wt). When the copolymerization of St and PMI was conducted using P(MTEA(S^+)[OTf^-]) macro-CTA at [AIBN]/[macro-CTA]/[St]/[PMI] = 1/5/1000/1000, a remarkable morphological change was detected by TEM. At an intermediate concentration (solid content = 10 wt%), tadpole-like structures including long worms with partially fused vesicles were visible after 0.5 h and 1 h, and then transformed into spherical vesicles at 3 h (Fig. 7a–c). DLS traces showed a gradual decrease in the size of the P(MTEA(S^+)[OTf^-])-*b*-P(St-*alt*-PMI) assemblies (D_h = 811, 492, and 170 nm after 0.5, 1, and 3 h, respectively) with an increase in the monomer conversion from 85% to 86%, and then 93%. Relatively lower zeta potentials of the P(MTEA(S^+)[OTf^-])-*b*-P(St-*alt*-PMI) assemblies were obtained after 0.5 and 1 h (14 and 6 mV), which may suggest the presence of unstable tadpole-like structures at those stages. These finally transformed to stable vesicle structures (zeta potential = 33 mV) after 3 h. These morphological changes using the P(MTEA(S^+)[OTf^-]) macro-CTA were substantially distinct from those using the P(MTEA(S^+)[$TFSI^-$]) macro-CTA. At a higher concentration (solid content = 20 wt%), P(MTEA(S^+)[OTf^-])-*b*-P(St-*alt*-PMI) self-assembled to afford sheet-like structures (Fig. 7d) in the early stage of PISA (0.5 h). As the hydrophobic P(St-*alt*-PMI) chain extended at longer polymerization times, the assemblies were transformed into long worms connected occasionally to the vesicles as an end-capping part (1 h), followed by long nanotubes (3 h), as confirmed by the TEM images (Fig. 7d–f, h, i). The length of the P(MTEA(S^+)[OTf^-])$_{48}$-*b*-P(St-*alt*-PMI)$_{223}$ nanotubes obtained after 3 h exceeded one micrometer (≥1 μm) with a diameter of 800–150 nm and a wall thickness of 20–40 nm. Relatively long

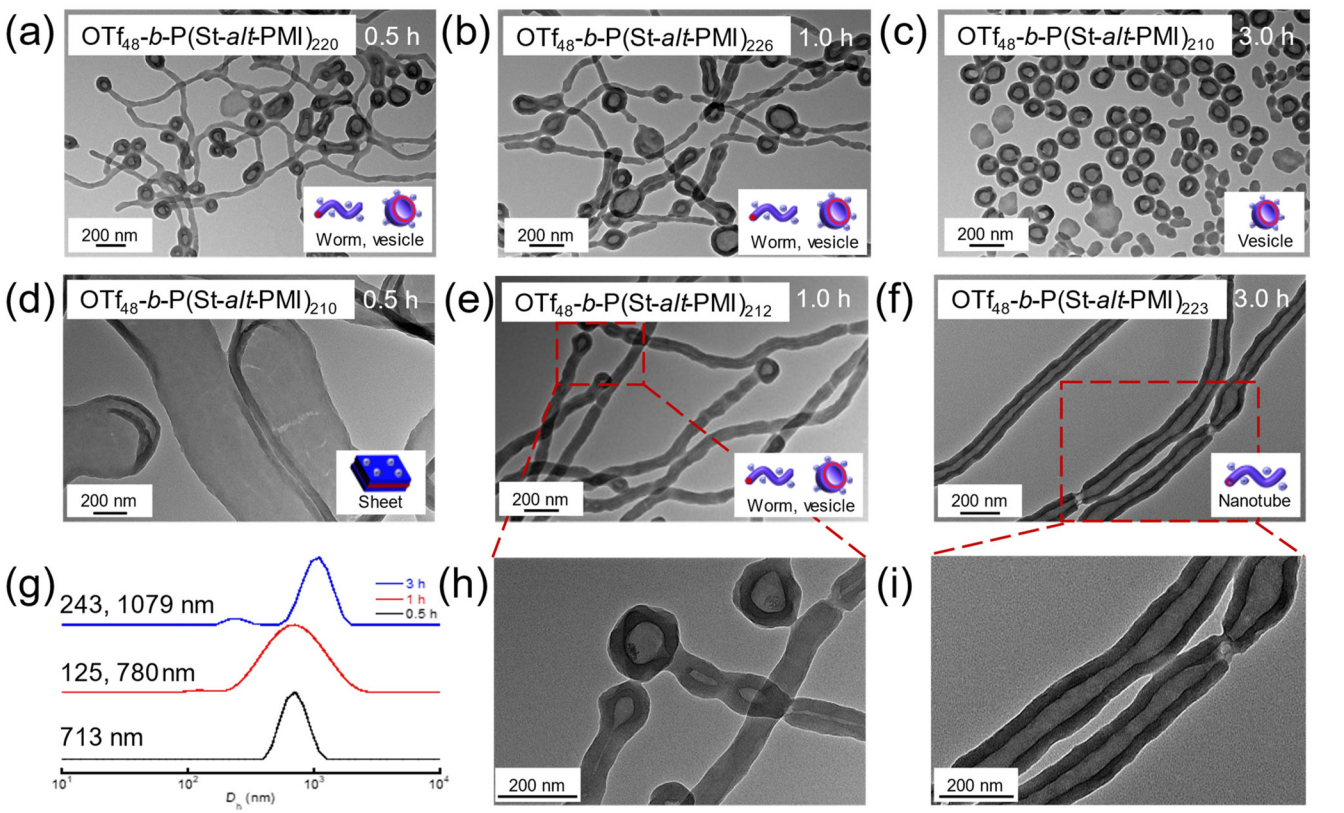

Fig. 7 (a–f, h and i) TEM images and (g) DLS measurements of P(MTEA(S^+)[OTf^-])-*b*-P(St-*alt*-PMI)s obtained by RAFT-PISA at [AIBN]/[macro-CTA]/[St]/[PMI] = 1/5/1000/1000, solvent = methanol : 1,4-dioxane = 7 : 3 at (a–c) 10 wt% and (d–i) 20 wt% using P(MTEA(S^+)[OTf^-]) macro-CTA (M_n = 15 200).

P(St-*alt*-PMI) blocks, compared to cationic P(MTEA(S^+)[R^-]), may lead to a high packing parameter, resulting in nanotube formation.[47] The breakage and partially connected parts were also visible along the nanotubes (Fig. 7i), implying that the nature of the cationic P(MTEA(S^+)[R^-]) had a limited impact on the brittleness of the nanotubes, and partial breakage was attributed to the rigid P(St-*alt*-PMI) segment. Under these conditions, the monomer conversion increased slightly with polymerization time (86, 93, and >99% for 0.5, 1, and 3 h, respectively), as monitored *via* ^{1}H NMR spectroscopy. Furthermore, the DP of the P(St-*alt*-PMI) segment, calculated from the sulfur content estimated by elemental analysis, increased slightly from 210 to 223, compared to 48 for P(MTEA(S^+)[OTf^-]) (Table S12†). DLS measurements of P(MTEA(S^+)[OTf^-])-*b*-P(St-*alt*-PMI)s indicated the presence of large assemblies (>700 nm), which increased with polymerization times (1 and 3 h), as shown in Fig. 7g. Two species with different sizes (243 nm and above 1000 nm) were detected in the P(MTEA(S^+)[OTf^-])-*b*-P(St-*alt*-PMI) assembly obtained after 3 h, suggesting the formation of nanotubes with large aspect ratios. Additionally, the zeta potential was approximately 35–40 mV and was independent of the polymerization time, implying the construction of cationic nano-objects with various morphologies, particularly nanotubes, which are covered with the cationic P(MTEA(S^+)[OTf^-]) block. Obviously, DLS is not suitable for accurate characterization of nanotube dispersions. Nevertheless, TEM image of the P(MTEA(S^+)[OTf^-])$_{48}$-*b*-P(St-*alt*-PMI)$_{233}$ assembly stained with OsO_4 solution showed the morphology with a hollow channel and dark wall (Fig. S22†), implying the formation of nanotube structures.

The P(MTEA(S^+)[Cl^-]) macro-CTA was then used for the copolymerization of St and PMI under the same conditions ([AIBN]/[macro-CTA]/[St]/[PMI] = 1/5/1000/1000, solid content = 20 wt% in methanol/1,4-dioxane (7/3, wt/wt), Table S16†), and almost monodisperse spherical micelles were obtained after 0.5 h (Fig. 8a). Subsequently, the assemblies underwent further structural changes to vesicles mixed with worms (1 h), then to large vesicles (3 h), as shown in Fig. 8b–d. An increase in the monomer conversion from 31% to 80% was observed with an increase in the DP of the P(St-*alt*-PMI) segment from 59 to 192 and the size (D_h) from 125 to 576 nm after 0.5 and 3 h, respectively. The zeta potential was approximately 29–38 mV. At lower concentrations (10 wt%) for 0.5 h (Fig. 8e), longer and thinner worms were formed, which were probably obtained by the connection of spherical micelles, as per a previously reported mechanism.[9] At longer polymerization times (1 and 3 h), worm structures were maintained, implying no further structural growth (Fig. S29† and 8e, f). Therefore, the assemblies obtained from the P(MTEA(S^+)[Cl^-]) macro-CTA underwent a spheres-to-worms-to-vesicles transition at a high concentration (20 wt%). Fig. 9 shows a phase diagrams constructed for P(MTEA(S^+)[R^-])-*b*-P(St-*alt*-PMI)s with different counter anions (R = TFSI, OTf, and Cl) prepared in methanol/1,4-dioxane = 7/3 (conc. = 20 wt%). This transition is governed by an increasing packing parameter *via* increasing solvophobic block length according to a general trend of the amphiphilic

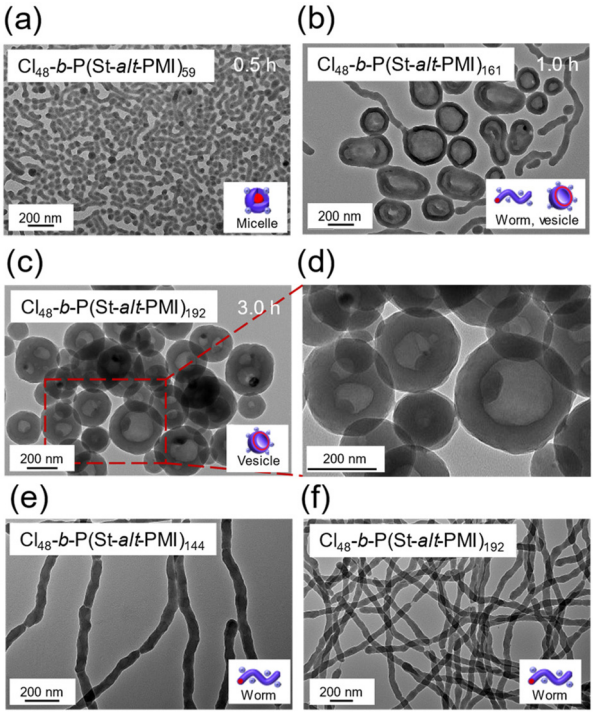

Fig. 8 (a–c) TEM images of P(MTEA(S^+)[Cl^-])-*b*-P(St-*alt*-PMI)s obtained by RAFT-PISA at [AIBN]/[macro-CTA]/[St]/[PMI] = 1/5/1000/1000 (solid content: (a–d) = 20 wt% and (e and f) = 10 wt%) using P(MTEA(S^+)[Cl^-]) macro-CTA (M_n = 9800) for (a and e) 0.5 h, (b) 1 h and (c, d and f) 3 h.

block copolymer, whereas limited structural evolution occurred at a lower concentration (10 wt%). These results suggest the formation of cationic nano-objects covered predominantly with the P(MTEA(S^+)[R^-]) chain, regardless of the counterion (R = TFSI, OTf, and Cl). The morphological transformation and resulting morphologies were affected by the nature of the P(MTEA(S^+)[R^-]) chain modulated by the counterions and the composition of the solvophilic/solvophobic blocks manipulated by the polymerization time and concentration (solid content in the feed). The calculated molecular weight of the P(MTEA(S^+)[Cl^-]) macro-CTA (M_n = 9800), based on the DP (48) of the pristine P(MTEA), was substantially lower than those of P(MTEA(S^+)[OTf^-]) (M_n = 15 200) and P(MTEA(S^+)[$TFSI^-$])(M_n = 21 500). This difference may also affect the volume fraction of the solvophilic block and the solvophilic/solvophobic balance, resulting in different assembled structures.

Formation of sulfonium nanotube-like structures with long hydrophobic chains

To verify the feasibility to form nanotube-like structures, we attempted to prepare P(MTEA(S^+)[R^-])-*b*-P(St-*alt*-PMI)s with extending the DP of the core forming block beyond 200, while maintaining the DP of the shell part (DP = 48). Initially, P(MTEA(S^+)[$TFSI^-$])-*b*-P(St-*alt*-PMI)s with longer hydrophobic chains were prepared at a higher monomer-to-CTA ratio ([AIBN]/[macro-CTA]/[St]/[PMI] = 1/5/1500/1500). As shown in

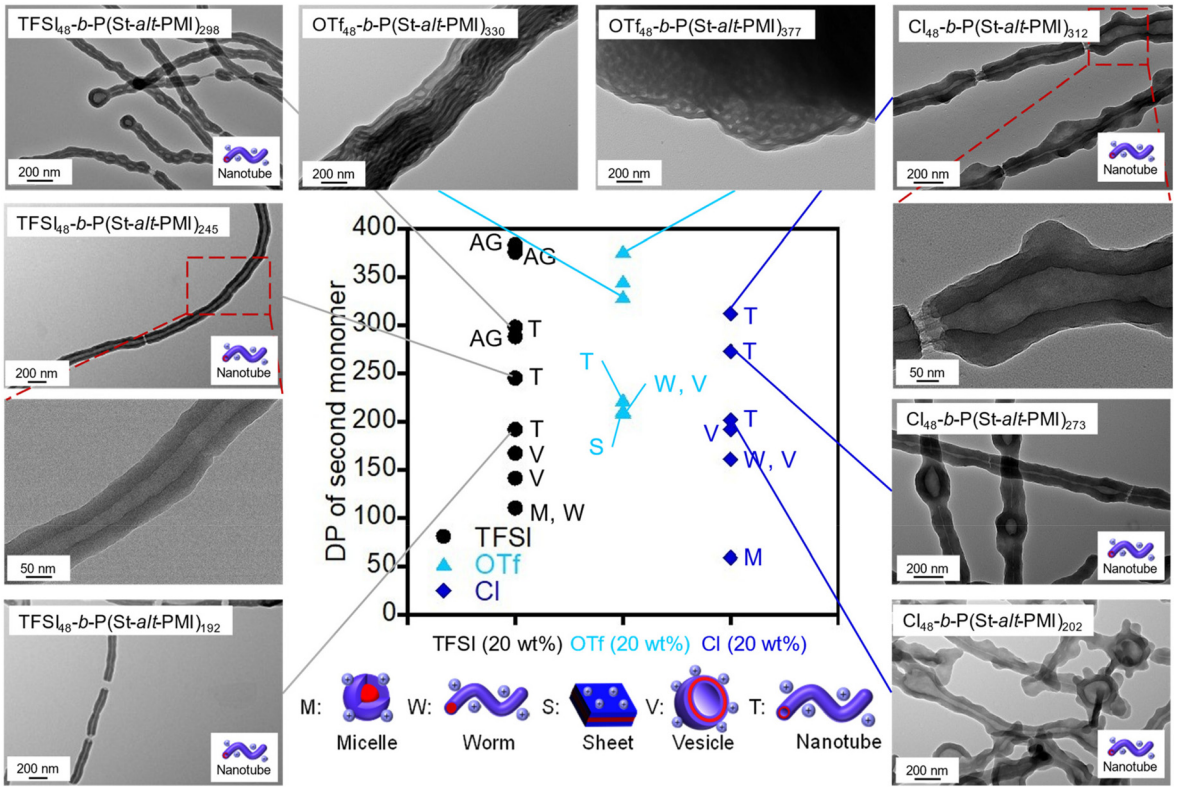

Fig. 9 Phase diagrams constructed for P(MTEA(S^+)[R^-])-*b*-P(St-*alt*-PMI)s with different counter anions (R = TFSI, OTf, and Cl) prepared in methanol/1,4-dioxane = 7/3 (conc. = 20 wt%). Morphology was determined by TEM, where M = micelle, W = worm, S = sheet, V = vesicle, T = nanotube, and AG = aggregates, respectively.

Fig. 9, P(MTEA(S^+)[$TFSI^-$])$_{48}$-*b*-P(St-*alt*-PMI)$_{192}$ and P(MTEA(S^+)[$TFSI^-$])$_{48}$-*b*-P(St-*alt*-PMI)$_{245}$ obtained after 0.5 and 1 h exhibited nanotube structures with uniform diameter and shell thickness. Nanotubes with partially broken and disconnected sections that adhered to each other to connect the two tubes were also observed (Fig. S31†). Similar nanotube-like structure was also observed, independent of staining (Fig. S32†). Nanotubes with many spherical vacant parts inside the tubes, shorter tubes with several disconnected points, and intermediated structures were observed for P(MTEA(S^+)[$TFSI^-$])$_{48}$-*b*-P(St-*alt*-PMI)$_{298}$, which was obtained after 3 h (Fig. 9 and S31, Table S17†). Using P(MTEA(S^+)[$TFSI^-$])$_{48}$, block copolymer nanotubes were observed over a relatively wide DP range of P(St-*alt*-PMI) from approximately 192 to 298. A further increase in the DP of the P(St-*alt*-PMI) blocks prepared at higher monomer-to-CTA ratios ([AINB]/[macro-CTA]/[St]/[PMI] = 1/5/2000/2000) led to the formation of aggregated structures with numerous pores (Fig. S33†). This behavior may be related to the mobility of the polymer chain because limited mobility was reported to be required to achieve a one-dimensional connection of the vesicles to afford nanotubes,[48] whereas high mobility leads to the three-dimensional fusion of vesicles and migration to afford large porous vesicles and assemblies consisting of many porous vesicles.

Similarly, block copolymer assemblies with longer hydrophobic P(St-*alt*-PMI) chains were prepared using P(MTEA(S^+)[OTf^-]) and P(MTEA(S^+)[Cl^-]) macro-CTAs at a high monomer-to-CTA ratio ([AIBNI]/[macro-CTA]/[St]/[PMI] = 1/5/1500/1500). Using P(MTEA(S^+)[OTf^-])$_{48}$, bangle-like structures formed by connecting the shell of several nanotubes, and three dimensional reticular structures consisting of many nanotubes were obtained with increasing the DP of P(St-*alt*-PMI) from 330 to 377 (Fig. 9 and S36, Table S18†). The nanotube structure was obtained only in the narrow DP range (roughly 200) for P(MTEA(S^+)[OTf^-])$_{48}$-*b*-P(St-*alt*-PMI)s. This is likely ascribed to the nature of P(MTEA(S^+)[OTf^-]), such as its ability to stick to each other and its limited solubility in methanol. For assemblies using P(MTEA(S^+)[Cl^-])$_{48}$, nanotube-like structures with a rough surface were obtained, which likely correspond to nanotubes with incorporated vesicles in the DP range of P(St-*alt*-PMI) from 202 to 312 (Fig. 9 and S38, Table S20†). Characteristic morphologies, which are probably cubosomes, were also observed for P(MTEA(S^+)[OTf^-])$_{48}$-*b*-P(St-*alt*-PMI)$_{377}$ (Fig. 9) and the same block copolymers with relatively long P(St-*alt*-PMI) chains (Fig. S23 and S25†). Further investigations are required to characterize such unique structures, which will be communicated separately. Therefore, the nature of the counter anion (R = TFSI, OTf, and Cl) of the sulfonium P(MTEA(S^+)[R^-]) macro-CTAs had a remarkable effect on the formation of stable nanotube structures with homogeneous three-dimensional structures and the practical range of the sol-

vophilic/solvophobic balance to afford characteristic nanotube structures.

Conclusion

Cationic block copolymer assemblies with tunable morphologies were developed *via* RAFT-PISA of St and PMI using three sulfonium macro-CTAs, P(MTEA(S^+)[$TFSI^-$]), P(MTEA(S^+)[OTf^-]), and P(MTEA(S^+)[Cl^-]). Positively charged nano-objects with various assemblies (*e.g.*, spheres, worms, vesicles, and nanotubes) were obtained for P(MTEA(S^+)[R^-])-*b*-P(St-*alt*-PMI)s, depending on the counterion (R = TFSI, OTf, and Cl) of the sulfonium macro-CTA. The assembled structures were governed by the adequate adjustment of the solvophilic/solvophobic block composition, P(St-*alt*-PMI) chain lengths tuned by the initial monomer-to-CTA feed ratios, solvent polarity (methanol/1,4-dioxane), monomer concentration (5–20 wt%), and polymerization time, in addition to the nature of the sulfonium cations tuned by the counter anion. Characteristic nanotube structures were produced by selecting suitable range of the solvophilic/solvophobic blocks and the nature of the sulfonium macro-CTA, enabling manipulation of the cationic charge of the nanotubes. This work not only proves the importance of the sulfonium macro-CTAs with different counter anions for constructing poly(ionic liquid)-based nanostructures but also demonstrates an efficient strategy for manipulating cationic functionalities and assembled structures *via* PISA and expanding the application potential.

Author contributions

Hirotsugu Miyakawa: investigation, methodology, writing – original draft. Hideharu Mori: conceptualization, supervision, validation, writing – review & editing.

Data availability

The data supporting this article have been included as part of the ESI.†

Conflicts of interest

There are no conflicts to declare.

Acknowledgements

This work was financially supported by a JSPS KAKENHI Grant-in-Aids for Scientific Research (B) (23H02007). We thank K. Mizuguchi for the help in the DOSY NMR measurement.

References

1 S. L. Canning, G. N. Smith and S. P. Armes, *Macromolecules*, 2016, **49**, 1985–2001.
2 J. Rieger, *Macromol. Rapid Commun.*, 2015, **36**, 1458–1471.
3 M. J. Derry, L. A. Fielding and S. P. Armes, *Prog. Polym. Sci.*, 2016, **52**, 1–18.
4 B. Charleux, G. Delaittre, J. Rieger and F. D'Agosto, *Macromolecules*, 2012, **45**, 6753–6765.
5 F. D'Agosto, J. Rieger and M. Lansalot, *Angew. Chem., Int. Ed.*, 2020, **59**, 8368–8392.
6 C. Liu, C.-Y. Hong and C.-Y. Pan, *Polym. Chem.*, 2020, **11**, 3673–3689.
7 X. Wang and Z. An, *Macromol. Rapid Commun.*, 2019, **40**, 1800325.
8 N. J. W. Penfold, J. Yeow, C. Boyer and S. P. Armes, *ACS Macro Lett.*, 2019, **8**, 1029–1054.
9 A. Blanazs, J. Madsen, G. Battaglia, A. J. Ryan and S. P. Armes, *J. Am. Chem. Soc.*, 2011, **133**, 16581–16587.
10 X. Zhang, S. Boisse, W. Zhang, P. Beaunier, F. D'Agosto, J. Rieger and B. Charleux, *Macromolecules*, 2011, **44**, 4149–4158.
11 N. J. Warren and S. P. Armes, *J. Am. Chem. Soc.*, 2014, **136**, 10174–10185.
12 J.-T. Sun, C.-Y. Hong and C.-Y. Pan, *Polym. Chem.*, 2013, **4**, 873–881.
13 J.-T. Sun, C.-Y. Hong and C.-Y. Pan, *Soft Matter*, 2012, **8**, 7753–7767.
14 W.-M. Wan and C.-Y. Pan, *Macromolecules*, 2010, **43**, 2672–2675.
15 S. Sugihara, A. Blanazs, S. P. Armes, A. J. Ryan and A. L. Lewis, *J. Am. Chem. Soc.*, 2011, **133**, 15707–15713.
16 W.-J. Zhang, C.-Y. Hong and C.-Y. Pan, *Macromolecules*, 2014, **47**, 1664–1671.
17 C. Gao, H. Zhou, Y. Qu, W. Wang, H. Khan and W. Zhang, *Macromolecules*, 2016, **49**, 3789–3798.
18 P. Gao, H. Cao, Y. Ding, M. Cai, Z. Cui, X. Lu and Y. Cai, *ACS Macro Lett.*, 2016, **5**, 1327–1331.
19 C. Gonzato, M. Semsarilar, E. R. Jones, F. Li, G. J. P. Krooshof, P. Wyman, O. O. Mykhaylyk, R. Tuinier and S. P. Armes, *J. Am. Chem. Soc.*, 2014, **136**, 11100–11106.
20 X. Zhang, J. Rieger and B. Charleux, *Polym. Chem.*, 2012, **3**, 1502–1509.
21 C. A. Figg, R. N. Carmean, K. C. Bentz, S. Mukherjee, D. A. Savin and B. S. Sumerlin, *Macromolecules*, 2017, **50**, 935–943.
22 D. Le, D. Keller and G. Delaittre, *Macromol. Rapid Commun.*, 2019, **40**, 1800551.
23 M. Semsarilar, V. Ladmiral, A. Blanazs and S. P. Armes, *J. Am. Chem. Soc.*, 2013, **29**, 7416–7424.
24 M. Williams, N. J. W. Penfold, J. R. Lovett, N. J. Warren, C. W. I. Douglas, N. Doroshenko, P. Verstraete, J. Smets and S. P. Armes, *Polym. Chem.*, 2016, **7**, 3864–3873.
25 V. Baddam, L. Valinen and H. Tenhu, *Macromolecules*, 2021, **54**, 4288–4299.

26 V. Baddam, L. Valinen, L. Kuckling and H. Tenhu, *Polym. Chem.*, 2022, **13**, 3790–3799.
27 B. Zhang, X. Yan, P. Alcouffe, A. Charlot, E. Fleury and J. Bernard, *ACS Macro Lett.*, 2015, **4**, 1008–1011.
28 J. Depoorter, X. Yan, B. Zhang, G. Sudre, A. Charlot, E. Fleury and J. Bernard, *Polym. Chem.*, 2021, **12**, 82–91.
29 C. Liu, S. Wang, H. Zhou, C. Gao and W. Zhang, *J. Polym. Sci., Part A: Polym. Chem.*, 2016, **54**, 945–954.
30 X. Xie, C. Liu, P. Cao, L. Qian, X. Meng, Z. Dai and Y. Xiong, *Polymer*, 2023, **285**, 126371.
31 J. Demarteau, A. Fernandez de Anastro, A. S. S. Shaplov and D. Mecerreyes, *Polym. Chem.*, 2020, **11**, 1481–1488.
32 D. Cordella, A. Debuigne, C. Jerome, Z. Kochovski, D. Taton and C. Detrembleur, *Macromol. Rapid Commun.*, 2016, **37**, 1181–1187.
33 D. Cordella, F. Ouhib, A. Aqil, T. Defize, C. Jerome, A. Serghei, E. Drockenmuller, K. Aissou, D. Taton and C. Detrembleur, *ACS Macro Lett.*, 2017, **6**, 121–126.
34 X. Pan, Z. Kochovski, Y.-L. Wang, R. M. Sarhan, E. Haerk, S. Gupta, S. Stojkovikj, G. A. El-Nagar, M. T. Mayer, R. Schuermann, J. Deumer, C. Gollwitzer, J. Yuan and Y. Lu, *J. Colloid Interface Sci.*, 2023, **637**, 408–420.
35 Y. Yang, J. Zheng, S. Man, X. Sun and Z. An, *Polym. Chem.*, 2018, **9**, 824–827.
36 Y. Yang, X. Li, Y. Yan, R. Pan, J. Liu, M. Lian, X. Luo and G. Liu, *e-Polymers*, 2022, **22**, 803–808.
37 J. Yuan, D. Mecerreyes and M. Antonietti, *Prog. Polym. Sci.*, 2013, **38**, 1009–1036.
38 J.-H. Choi, Y. Ye, Y. A. Elabd and K. I. Winey, *Macromolecules*, 2013, **46**, 5290–5300.
39 E. Margaretta, G. B. Fahs, J. Inglefield, L. David, C. Jangu, D. Wang, J. R. Heflin, R. B. Moore and T. E. Long, *ACS Appl. Mater. Interfaces*, 2016, **8**, 1280–1288.
40 B. Wu, W. Zhang, N. Gao, M. Zhou, Y. Liang, Y. Wang, F. Li and G. Li, *Sci. Rep.*, 2017, **7**, 13973.
41 H. He, K. Rahimi, M. Zhong, A. Mourran, D. R. Luebke, H. B. Nulwala, M. Moeller and K. Matyjaszewski, *Nat. Commun.*, 2017, **8**, 14057.
42 H. Luo, Q. Tang, J. Zhong, Z. Lei, J. Zhou and Z. Tong, *Macromol. Chem. Phys.*, 2019, **220**, 1800508.
43 K. Vijayakrishna, S. K. Jewrajka, A. Ruiz, R. Marcilla, J. A. Pomposo, D. Mecerreyes, D. Taton and Y. Gnanou, *Macromolecules*, 2008, **41**, 6299–6308.
44 K. Vijayakrishna, D. Mecerreyes, Y. Gnanou and D. Taton, *Macromolecules*, 2009, **42**, 5167–5174.
45 Y. Mai and A. Eisenberg, *Chem. Soc. Rev.*, 2012, **41**, 5969–5985.
46 X. Chen, L. Liu, M. Huo, M. Zeng, L. Peng, A. Feng, X. Wang and J. Yuan, *Angew. Chem., Int. Ed.*, 2017, **56**, 16541–16545.
47 Z. Ding, M. Ding, C. Gao, C. Boyer and W. Zhang, *Macromolecules*, 2017, **50**, 7593–7602.
48 F. Lv, Z. An and P. Wu, *Macromolecules*, 2020, **53**, 367–373.
49 C. Kumano, H. Miyakawa, K. Masuko and H. Mori, *Polym. Chem.*, 2024, **15**, 2397–2407.
50 R.-M. Zhu, Z.-X. Chang, W.-J. Zhang and C.-Y. Hong, *Macromolecules*, 2023, **56**, 3296–3303.
51 S. Varlas, R. Keogh, Y. Xie, S. L. Horswell, J. C. Foster and R. K. O'Reilly, *J. Am. Chem. Soc.*, 2019, **141**, 20234–20248.
52 Q. Zhang, R. Zeng, Y. Zhang, Y. Chen, L. Zhang and J. Tan, *Macromolecules*, 2020, **53**, 8982–8991.
53 X.-F. Xu, R.-M. Zhu, C.-Y. Pan, Y.-Z. You, W.-J. Zhang and C.-Y. Hong, *Macromolecules*, 2021, **54**, 2729–2739.
54 A. Bhattacharjee, A. Luis, J. H. Santos, J. A. Lopes-da-Silva, M. G. Freire, P. J. Carvalho and J. A. P. Coutinho, *Fluid Phase Equilib.*, 2014, **381**, 36–45.
55 H. Matsumoto, T. Matsuda and Y. Miyazaki, *Chem. Lett.*, 2000, **12**, 1430–1431.
56 A. J. R. Rennie, V. L. Martins, R. M. Torresi and P. J. Hall, *J. Phys. Chem. C*, 2015, **119**, 23865–23874.
57 X. Baokou and M. Anouti, *J. Phys. Chem. C*, 2015, **119**, 970–979.
58 E. Coadou, P. Goodrich, A. R. Neale, L. Timperman, C. Hhardacre, J. Jacquemin and M. Anouti, *ChemPhysChem*, 2016, **17**, 3992–4002.
59 M. C. Mackenzie, A. R. Shrivats, D. Konkolewicz, S. E. Ayerick, M. C. McDermott, J. O. Hollinger and K. Matyjaszewski, *Biomacromolecules*, 2015, **16**, 236–245.
60 S. T. Hemp, M. H. Allen, Jr., A. E. Smith and T. E. Long, *ACS Macro Lett.*, 2013, **2**, 731–735.
61 J. R. Kramer and T. J. Deming, *Biomacromolecules*, 2012, **13**, 1719–1723.
62 X. Wang, G. Wang, J. Zhao, Z. Zhu and J. Rao, *ACS Macro Lett.*, 2021, **10**, 1643–1649.
63 D. Cordella, A. Kermagoret, A. Debuigne, C. Jerome, D. Mecerreyes, M. Isik, D. Taton and C. Detrembleur, *Macromolecules*, 2015, **48**, 5230–5243.
64 J. Texter, *Macromol. Rapid Commun.*, 2012, **33**, 1996–2014.
65 E. Karjalainen, V. Aseyev and H. Tenhu, *Macromolecules*, 2014, **47**, 7581–7587.
66 V. Baddam, R. Missonen, S. Hietala and H. Tenhu, *Macromolecules*, 2019, **52**, 6514–6522.
67 M. A. Morris, H. An, J. L. Lutkenhaus and T. H. Epps, III, *ACS Energy Lett.*, 2017, **2**, 1919–1936.
68 A. J. Peltekoff, S. Brixi, J. Niskanen and B. H. Lessard, *JACS Au*, 2021, **1**, 1044–1056.
69 D. N. M. Kusmus, T. v. Veldhuisen, S. Michel-Souzy, J. J. L. M. Cornelissen and J. M. J. Paulusse, *RSC Appl. Polym.*, 2024, **2024**, 678–691.
70 P. Yang, L. P. D. Ratcliffe and S. P. Armes, *Macromolecules*, 2013, **46**, 8545–8556.